INSTITUTE OF PHYSICS PUBLISHING JOURNAL OF PHYSICS B: ATOMIC, MOLECULAR AND OPTICAL PHYSICS

J. Phys. B: At. Mol. Opt. Phys. **34** (2001) 915–931 www.iop.org/Journals/jb PII: S0953-4075(01)18456-7

# Multiconfiguration Dirac–Hartree–Fock calculations of the forbidden transitions between $3s^2\ ^1S_0$, $3s3p\ ^3P_{0,1,2}$, $^1P_1$ states for Mg-like ions

**Yu Zou and C Froese Fischer**

Department of Electrical Engineering and Computer Science, Box 1679 B, Vanderbilt University, Nashville, TN 37235, USA

Received 30 October 2000, in final form 10 January 2001

**Abstract**

Weak forbidden transitions are of great interest for plasma diagnostics, but they are sensitive to many factors in theoretical calculations. In earlier work on the intercombination transition using the multiconfiguration Dirac–Hartree–Fock approach for $Al^+$–$S^{4+}$ ions, a method was developed to eliminate the dependence of the transition rates on the optimization strategy. In this paper, this method is applied to other $LS$ forbidden transitions. For the $LS$ allowed transitions the transition energy normalization can eliminate such a dependence. It is also found that the fine structure splittings corrected by the non-relativistic limit offsets are independent of optimization strategies and are in good agreement with observations. For the high-$Z$ ions, the dependence on strategies is less important and the calculations for all the transitions (E1, E2, M1, M2) are extended to $Z = 92$. A general scaling formula is adopted to reduce the extensive variation of the rates with respect to the nuclear charge.

## 1. Introduction

Atomic radiative transitions are one of the fundamental processes in plasmas. The numerical simulation of atomic kinetics in laboratory as well as astrophysical plasmas requires numerous accurate radiative transition rates. The atomic kinetics primarily depends on optical allowed transitions. However, weak forbidden transitions are of great interest for the plasma diagnostics since the photons from such transitions may carry information from large optical depths within the plasma [1].

The rates of the optical allowed transitions can be calculated quite accurately by various theories. However, weak forbidden transitions are sensitive to many factors, e.g. electron correlation, relativistic effects including the Breit interaction. In the earlier work on the $Al^+$ to $S^{4+}$ ions [2], it was found that the *ab initio* rates of intercombination transitions depended on the optimization strategy of orbitals in the multiconfiguration Dirac–Hartree–Fock calculations. The non-relativistic (NR) limit correction [3] and energy normalizations [4, 5] were required to achieve identical results for different strategies.

In this paper, the method is applied to the M1, E2 and M2 transitions in the Mg isoelectronic sequence. For the $LS$ allowed transitions which have non-zero rates at the non-relativistic limit where $LS$ are good quantum numbers, only the transition energy normalization is necessary to eliminate the sensitivity on optimization strategies. For the $LS$ forbidden transitions in which the rate should vanish at the NR limit, both the NR limit correction and the energy normalizations are necessary to eliminate the dependence on optimization strategies. Generally, the atomic radiative transition rates depend strongly on the nuclear charge, especially for forbidden transitions. A general scaling formula is adopted to reduce the extensive variation of transition rates with respect to the nuclear charge.

## 2. Computational procedures

The graspVU code, a modified version of GRASP92 [6], is used to calculate the wavefunctions of the atomic system and the transition matrix elements. The same expansions are adopted as in the earlier work [2] on the intercombination transitions. The valence correlation and the 2s, 2p core–valence correlations are taken into account for both upper and lower states of the transitions. Under such expansions, the multiconfiguration Dirac–Hartree–Fock (MCDHF) approach is adopted to obtain the radial orbitals and mixing coefficients simultaneously. Then the configuration-interaction procedure is performed to take into account the Breit interaction.

A test calculation is performed for $Al^+$, $Mo^{30+}$ and $U^{80+}$ to estimate the effect of the Breit interaction. Although the Breit interaction only has a small effect on transition matrix elements except for the $LS$ forbidden transitions of low-$Z$ ions, it affects transition energies by about 6%, 2% and 1% for $Al^+$, $Mo^{30+}$ and $U^{80+}$, respectively. The transition rates may be affected correspondingly more since the rate is proportional to $\Delta E^{2\kappa+1}$, where in the present work $\kappa = 1$ or 2. Consequently, the Breit interaction is included throughout the work.

The finite-nucleus effect is taken into account by assuming an extended Fermi distribution for the nucleus. Since the orbitals for the upper and lower states of a transition may be obtained by separate optimizations, the biorthonormal technique [7, 8] is applied to make the orbitals biorthonormal and then the standard Racah algebra can be used in the calculations of transition matrix elements.

Paralleling the normal MCDHF calculations the non-relativistic limit calculations are carried out by setting the speed of light to $10^5$ au in order to obtain the NR offsets for fine structure splittings as well as transition matrix elements of $LS$ forbidden transitions.

At the NR limit, the radial part of the matrix element of an electric multipole transition in the Babushkin gauge can be expressed as [9]

$$\bar{M}^e_{ij}(\kappa) = B(e)\Delta E^\kappa \int_0^\infty R_i R_j r^\kappa \, \mathrm{d}r \tag{1}$$

where $\Delta E$ is the transition energy. Similarly, that of a magnetic multipole can be written as

$$\bar{M}^m_{ij}(\kappa) = B(m)\Delta E^\kappa \int_0^\infty R_i R_j r^{\kappa-1} \, \mathrm{d}r. \tag{2}$$

Therefore, we define the radiative element with the NR limit correction for the $LS$ forbidden transition as

$$M^C = \left[ \frac{M^R}{(\Delta E^R)^\kappa} - \frac{M^{NR}}{(\Delta E^{NR})^\kappa} \right] (\Delta E^R)^\kappa \tag{3}$$

where $M^R$ is the radiative matrix element from MCDHF + CI wavefunctions and $M^{NR}$ is the corresponding NR offset. The transition rate with the NR limit correction is

$$A'_{ji} = \frac{0.667\,02}{g_i}\Delta E^2\ (\mathrm{cm}^{-1})gf \tag{4}$$

where

$$gf = \frac{g_j}{2\kappa+1}\frac{c^2}{\Delta E}(M^C_{ij})^2. \tag{5}$$

With the accurate experimental transition energy the transition rate can be normalized so that

$$A'' = A'\left(\frac{E^e}{E^R}\right)^{2\kappa+1} \tag{6}$$

where $E^e$ is the accurate experimental energy. This transition energy normalization can be applied to both $LS$ allowed and $LS$ forbidden transitions. Since the $^1P_1$ component converges slowly with respect to $l$, a singlet–triplet normalization [4, 5] is adopted for $LS$ forbidden transitions, so that

$$A''' = A''\left[\frac{E^R(^1\mathrm{P}) - E^R(^3\mathrm{P})}{E^e(^1\mathrm{P}) - E^e(^3\mathrm{P})}\right]^2. \tag{7}$$

The singlet–triplet normalization can be derived from first-order perturbation theory. Assuming approximation state functions of $^3P_1$ and $^1P_1$ can be expanded in the $LSJ$ representation as

$$\Psi(^3\mathrm{P}_1) = a\Phi(^3\mathrm{P}_1) + b\Phi(^1\mathrm{P}_1)$$
$$\Psi(^1\mathrm{P}_1) = a'\Phi(^3\mathrm{P}_1) + b'\Phi(^1\mathrm{P}_1).$$

The coefficients $b, a'$ are proportional to $1/[E(^1\mathrm{P}_1) - E(^3\mathrm{P}_1)]$ according to the first-order perturbation theory. And the radiative matrix element of the $LS$ forbidden transition is proportional to $b$ or $a'$. In the special case of the $LS$ forbidden transition between the $^3P_1$ state and the $^1P_1$ state, the element is proportional to the linear combination of $b$ and $a'$. Therefore, the singlet–triplet normalization is still applicable. This normalization is valid when the first-order theory is suitable.

## 3. Results and discussions

The optimization strategy for the ground state of $3s^2\ ^1S_0$ is for the single state since the admixture of $3p^2\ ^3P_0$ is unimportant in this case. For the odd-parity states of 3s3p, four optimization strategies in table 1 are used for the $Al^+$ ion in the MCDHF calculation. For all the strategies, the $n \leqslant 3$ orbitals are optimized to the functional of the linear combination of $3s3p\ ^3P_{0,1,2}$ states with $2J + 1$ as their weights. In strategy I, the optimization is performed on the $3s3p\ ^3P_{0,1,2}$ eigenstates with statistical weights for the $n = 4$–7 orbitals. In strategy II, an additional $^1P_1$ eigenstate is included. Strategy III has the same eigenstates as strategy II but equal weights are used instead of statistical ones. In strategy IV, the $n = 4$ orbitals are optimized to the $3s3p\ ^3P_{0,1,2}$, $^1P_1$ eigenstates with statistical weights and the $n = 5$–7 orbitals only to the $3s3p\ ^3P_1$, $^1P_1$ eigenstates. For the 7g active set of orbitals, the numbers of CSFs in the $0^+$, $0^-$, $1^-$ and $2^-$ symmetries are 2552, 3974, 10 872 and 15 008, respectively.

Table 2 shows the energies and rates of the $LS$ allowed M1, E2 and M2 transitions for the $Al^+$ ion using the four strategies. The M2 transition $3s^2\ ^1S_0$–$3s3p\ ^3P_2$ is an $LS$ allowed transition since the M2 operator is a spin-changing one. The $\Delta E^R$ is the *ab initio* transition

**Table 1.** The optimization strategies for the odd-parity states of the $Al^+$ ion in MCDHF calculations.

| Strategy | I | | II | | III | | IV | |
|---|---|---|---|---|---|---|---|---|
| AS | Eigenstate | Weight | Eigenstate | Weight | Eigenstate | Weight | Eigenstate | Weight |
| 3d | $^3P^o_{0,1,2}$ | $2J+1$ | $^3P^o_{0,1,2}$ | $2J+1$ | $^3P^o_{0,1,2}$ | $2J+1$ | $^3P^o_{0,1,2}$ | $2J+1$ |
| 4f | $^3P^o_{0,1,2}$ | $2J+1$ | $^3P^o_{0,1,2}$, $^1P^o_1$ | $2J+1$ | $^3P^o_{0,1,2}$, $^1P^o_1$ | 1 | $^3P^o_{0,1,2}$, $^1P^o_1$ | $2J+1$ |
| 5g | $^3P^o_{0,1,2}$ | $2J+1$ | $^3P^o_{0,1,2}$, $^1P^o_1$ | $2J+1$ | $^3P^o_{0,1,2}$, $^1P^o_1$ | 1 | $^3P^o_1$, $^1P^o_1$ | 1 |
| 6g | $^3P^o_{0,1,2}$ | $2J+1$ | $^3P^o_{0,1,2}$, $^1P^o_1$ | $2J+1$ | $^3P^o_{0,1,2}$, $^1P^o_1$ | 1 | $^3P^o_1$, $^1P^o_1$ | 1 |
| 7g | $^3P^o_{0,1,2}$ | $2J+1$ | $^3P^o_{0,1,2}$, $^1P^o_1$ | $2J+1$ | $^3P^o_{0,1,2}$, $^1P^o_1$ | 1 | $^3P^o_1$, $^1P^o_1$ | 1 |

**Table 2.** The energies (in $cm^{-1}$) and rates (in $s^{-1}$) of M1, E2 and M2 transitions for the $Al^+$ ion calculated with different optimization strategies. $A_N$ represents the normalized rate, $A_N = (\Delta E^e/\Delta E)^{2\kappa+1} A$. For the E2 transitions the Babushkin gauge is adopted. $\Delta E^R$ is the *ab initio* transition energy. $\Delta E^C$ is the corrected value, $\Delta E^C = \Delta E^R - \Delta E^{NR}$, where $\Delta E^{NR}$ is the corresponding NR offset.

| Strategy | I | II | III | IV | Expt |
|---|---|---|---|---|---|
| 3s3p $^3P_0$–3s3p $^3P_1$ (M1) | | | | | |
| $\Delta E^R$ | 60.49 | 60.56 | 62.79 | 61.43 | 60.88 |
| $\Delta E^C$ | 60.43 | 60.48 | 60.48 | 60.48 | |
| $A$ | 3.980(−6) | 3.994(−6) | 4.452(−6) | 4.169(−6) | |
| $A_N$ | 4.061(−6) | 4.062(−6) | 4.061(−6) | 4.061(−6) | |
| 3s3p $^3P_1$–3s3p $^3P_2$ (M1) | | | | | |
| $\Delta E^R$ | 123.2 | 123.3 | 127.8 | 125.1 | 123.9 |
| $\Delta E^C$ | 123.1 | 123.1 | 123.2 | 123.2 | |
| $A$ | 2.518(−5) | 2.529(−5) | 2.818(−5) | 2.639(−5) | |
| $A_N$ | 2.565(−5) | 2.565(−5) | 2.565(−5) | 2.565(−5) | |
| 3s3p $^3P_0$–3s3p $^3P_2$ (E2) | | | | | |
| $\Delta E^R$ | 183.6 | 183.9 | 190.6 | 186.5 | 184.8 |
| $\Delta E^C$ | 183.4 | 183.7 | 183.7 | 183.7 | |
| $A_B$ | 1.796(−10) | 1.810(−10) | 2.168(−10) | 1.944(−10) | |
| $A_C$ | 1.980(−10) | 1.869(−10) | 2.400(−10) | 2.054(−10) | |
| $A_N$ | 1.856(−10) | 1.856(−10) | 1.856(−10) | 1.857(−10) | |
| 3s3p $^3P_1$–3s3p $^3P_2$ (E2) | | | | | |
| $\Delta E^R$ | 123.2 | 123.3 | 127.8 | 125.1 | 123.9 |
| $\Delta E^C$ | 123.1 | 123.1 | 123.2 | 123.2 | |
| $A_B$ | 5.484(−11) | 5.527(−11) | 6.620(−11) | 5.938(−11) | |
| $A_C$ | 6.041(−11) | 5.701(−11) | 7.330(−11) | 6.277(−11) | |
| $A_N$ | 5.653(−11) | 5.661(−11) | 5.661(−11) | 5.663(−11) | |
| $3s^2$ $^1S_0$–3s3p $^3P_2$ (M2) | | | | | |
| $\Delta E^R$ | 37 575 | 37 634 | 37 642 | 37 668 | 37 578 |
| $A$ | 3.411(−3) | 3.439(−3) | 3.442(−3) | 3.454(−3) | |
| $A_N$ | 3.412(−3) | 3.413(−3) | 3.413(−3) | 3.413(−3) | |

energy. For the fine structure transitions, $\Delta E^C$ is the corrected value by $\Delta E^C = \Delta E^R - \Delta E^{NR}$, where $\Delta E^{NR}$ is the NR offset of the transition energy. The *ab initio* transition energies between the fine structure levels of $^3P$ depend on the strategies to some extent. The energy offsets for strategies I and II are very small because the statistical weights are used and the optimization involves all the states in $^3P$. For strategy III the offsets are larger because equal weights are used instead of statistical ones and for strategy IV because the $^3P_{0,2}$ eigenstates are not included

**Table 3.** The energies (in $cm^{-1}$), radiative elements (in au) and rates (in $s^{-1}$) for M1 and E2 transitions of $3s3p\ ^3P_J$–$3s3p\ ^1P_1$ for the $Al^+$ ion calculated with different optimization strategies. $M^R$ is the *ab initio* radiative element and $M^{NR}$ is the corresponding NR offset. $A$ represents the *ab initio* rates from MCDHF, $A'$ with the NR offset subtracted, $A''$ with the transition energy normalization and $A'''$ with the singlet–triplet normalization. For brevity, four rates are given for the first transition but only the final corrected rate $A'''$ is listed for all the transitions.

| Strategy | I | II | III | IV | Expt |
|---|---|---|---|---|---|
| $^3P_0$–$^1P_1$ (M1) | | | | | |
| $\Delta E$ | 23 081 | 22 820 | 22 823 | 22 743 | 22 459 |
| $M^R$ | 1.834(−8) | 1.833(−8) | 1.917(−8) | 1.856(−8) | |
| $M^{NR}$ | −1.589(−10) | −2.752(−11) | 8.270(−10) | 2.819(−10) | |
| $A$ | 2.372(−3) | 2.341(−3) | 2.562(−3) | 2.394(−3) | |
| $A'$ | 2.413(−3) | 2.348(−3) | 2.344(−3) | 2.322(−3) | |
| $A''$ | 2.223(−3) | 2.239(−3) | 2.234(−3) | 2.236(−3) | |
| $A'''$ | 2.348(−3) | 2.312(−3) | 2.307(−3) | 2.293(−3) | |
| $^3P_1$–$^1P_1$ (M1) | | | | | |
| $\Delta E$ | 23 020 | 22 760 | 22 760 | 22 681 | 22 398 |
| $M^R$ | −9.234(−9) | −9.232(−9) | −9.653(−9) | −9.350(−9) | |
| $M^{NR}$ | 8.070(−11) | 1.383(−11) | −4.139(−10) | −1.410(−10) | |
| $A'''$ | 1.781(−3) | 1.754(−3) | 1.751(−3) | 1.740(−3) | |
| $^3P_2$–$^1P_1$ (M1) | | | | | |
| $\Delta E$ | 22 897 | 22 636 | 22 632 | 22 556 | 22 274 |
| $M^R$ | 9.069(−9) | 9.058(−9) | 9.480(−9) | 9.179(−9) | |
| $M^{NR}$ | −7.868(−11) | −1.376(−11) | 4.145(−10) | 1.407(−10) | |
| $A'''$ | 2.846(−3) | 2.799(−3) | 2.797(−3) | 2.779(−3) | |
| $^3P_1$–$^1P_1$ (E2) | | | | | |
| $\Delta E$ | 23 020 | 22 760 | 22 760 | 22 681 | 22 398 |
| $M^R$ | −5.929(−9) | −5.971(−9) | −6.880(−9) | −6.835(−9) | |
| $M^{NR}$ | −1.641(−10) | −7.778(−11) | −9.557(−10) | −9.450(−10) | |
| $A'''$ | 3.872(−4) | 4.142(−4) | 4.179(−4) | 4.159(−4) | |
| $^3P_2$–$^1P_1$ (E2) | | | | | |
| $\Delta E$ | 22 897 | 22 636 | 22 632 | 22 556 | 22 274 |
| $M^R$ | 3.888(−9) | 3.641(−9) | 4.545(−9) | 4.632(−9) | |
| $M^{NR}$ | −5.528(−11) | −3.207(−10) | 5.326(−10) | 7.481(−10) | |
| $A'''$ | 3.002(−4) | 3.099(−4) | 3.188(−4) | 3.010(−4) | |

for the $n = 5$–7 orbitals. However, after the NR limit correction the fine structure splittings are nearly identical for all the strategies. No quantum electrodynamics (QED) corrections have been included in table 2, which may account for the small discrepancy in comparison with experiments. The deviations of the *ab initio* $A$ rates from different strategies are about 12%, 20% and 1% for the $LS$ allowed M1, E2 and M2 transitions, respectively. The $A_N$ represents the rate normalized by equation (6). For the E2 transitions the Babushkin gauge is adopted in the normalization. The normalized rates $A_N$ from different strategies are in excellent agreement with each other. For these $LS$ allowed transitions, the transition energy normalization eliminates the strategy dependence. This suggests that the transition element might be independent of the strategy but not the transition energy.

The energies, radiative elements and rates are shown in table 3 for the $LS$ forbidden M1 and E2 transitions of $3s3p\ ^3P_J$–$3s3p\ ^1P_1$ for the $Al^+$ ion calculated with different optimization strategies. The $M^R$ is the *ab initio* radiative element and $M^{NR}$ is the corresponding NR offset. Generally, strategies III and IV give larger NR offsets because of the equal weights and

**Table 4.** The energies (in $cm^{-1}$) and rates (in $s^{-1}$) of M1 and E2 transitions between the levels of 3s3p $^3P_{0,1,2}$ for the $Al^+$, $Si^{2+}$, $P^{3+}$ and $S^{4+}$ ions calculated with strategy IV. $A_N$ represents the normalized rate $A_N = (\Delta E^e/\Delta E)^{2\kappa+1}\,A$. For the E2 transitions the Babushkin gauge is adopted. $\Delta E^R$ is the *ab initio* transition energy. $\Delta E^C$ is the corrected value, $\Delta E^C = \Delta E^R - \Delta E^{NR}$, where $\Delta E^{NR}$ is the corresponding NR offset.

| | $Al^+$ | $Si^{2+}$ | $P^{3+}$ | $S^{4+}$ |
|---|---|---|---|---|
| $^3P_0$–$^3P_1$ (M1) | | | | |
| $\Delta E^e$ | 60.88 | 128.6 | 227.4 | 369.5 |
| $\Delta E^R$ | 61.43 | 129.9 | 229.3 | 369.1 |
| $\Delta E^C$ | 60.48 | 128.5 | 227.4 | 367.4 |
| $A$ | 4.169(−6) | 3.851(−5) | 2.169(−4) | 9.040(−4) |
| $A_N$ | 4.061(−6) | 3.771(−5) | 2.103(−4) | 9.069(−4) |
| $^3P_1$–$^3P_2$ (M1) | | | | |
| $\Delta E^e$ | 123.9 | 261.7 | 468.4 | 761.9 |
| $\Delta E^R$ | 125.1 | 263.6 | 471.5 | 764.0 |
| $\Delta E^C$ | 123.2 | 260.8 | 467.6 | 760.6 |
| $A$ | 2.639(−5) | 2.469(−4) | 1.413(−3) | 6.013(−3) |
| $A_N$ | 2.565(−5) | 2.398(−4) | 1.386(−3) | 5.963(−3) |
| $^3P_0$–$^3P_2$ (E2) | | | | |
| $\Delta E^e$ | 184.8 | 390.3 | 695.8 | 1131 |
| $\Delta E^R$ | 186.5 | 392.5 | 700.8 | 1133 |
| $\Delta E^C$ | 183.7 | 388.2 | 695.0 | 1128 |
| $A_B$ | 1.944(−10) | 3.009(−9) | 2.591(−8) | 1.557(−7) |
| $A_C$ | 2.054(−10) | 3.058(−9) | 2.616(−8) | 1.576(−7) |
| $A_N$ | 1.857(−10) | 2.878(−9) | 2.499(−8) | 1.542(−7) |
| $^3P_1$–$^3P_2$ (E2) | | | | |
| $\Delta E^e$ | 123.9 | 261.7 | 468.4 | 761.9 |
| $\Delta E^R$ | 125.1 | 263.6 | 471.5 | 764.0 |
| $\Delta E^C$ | 123.2 | 260.8 | 467.6 | 760.6 |
| $A_B$ | 5.937(−11) | 9.255(−10) | 8.041(−9) | 4.886(−8) |
| $A_C$ | 6.277(−11) | 9.416(−10) | 8.128(−9) | 4.934(−8) |
| $A_N$ | 5.663(−11) | 8.811(−10) | 7.779(−9) | 4.818(−8) |

the incomplete eigenstates in the optimization, consistent with the finding for fine structure splittings. $A$ represents the *ab initio* rates from MCDHF, $A'$ with the NR offset subtracted, $A''$ with the transition energy normalization and $A'''$ with the singlet–triplet normalization. For brevity, different rates are given only for the first transition and only the final corrected rate $A'''$ is listed for all the transitions. The deviation for the *ab initio* rates is about 9% for M1 transitions and 28%, 44% for the two E2 transitions, respectively. With the NR limit correction the agreement improves substantially for the E2 transitions. Since strategy I does not include the eigenstate $^1P_1$ it gets poor agreement with other strategies after the transition energy normalization. Finally, with the singlet–triplet normalization, the deviations are reduced to about 2% for M1 transitions and 8%, 6% for the E2 transitions.

Since the results are nearly independent of the optimization strategies, the most efficient strategy, namely, strategy IV, is adopted to calculate the ions along the Mg iso-electronic sequence. Table 4 shows the results for the transitions between the fine structure levels of 3s3p $^3P$ for the lowest four ions in the sequence. The fine structure splittings corrected with the corresponding NR offset are in good agreement with those of experiments. The NR offsets are nearly constant for different ions, whereas the fine structure splittings increase rapidly as the nuclear charge increases. Consequently, the NR offset correction to fine structure splittings

**Table 5.** The energies (in $cm^{-1}$), radiative elements (in au) and rates (in $s^{-1}$) for the M1 and E2 transitions of $3s3p\ ^3P_J$–$3s3p\ ^1P_1$ for the $Al^+$, $Si^{2+}$, $P^{3+}$ and $S^{4+}$ ions calculated with strategy IV. $M^R$ is the *ab initio* radiative element and $M^{NR}$ is the corresponding NR offset. $A$ represents the *ab initio* rates from the MCDHF + CI approach, $A'$ with the NR offset subtracted, $A''$ with the transition energy normalization and $A'''$ with the singlet–triplet normalization. For brevity, four rates are given for the first transition but only the final corrected rate $A'''$ is listed for all the transitions.

| | $Al^+$ | $Si^{2+}$ | $P^{3+}$ | $S^{4+}$ |
|---|---|---|---|---|
| $^3P_0$–$^1P_1$ (M1) | | | | |
| $E^e$ | 22 459 | 30 159 | 37 277 | 44 126 |
| $E^R$ | 22 743 | 30 428 | 37 542 | 44 395 |
| $M^R$ | 1.856(−8) | 4.182(−8) | 7.697(−8) | 1.267(−7) |
| $M^{NR}$ | 2.819(−10) | 4.791(−10) | 6.556(−10) | 6.155(−10) |
| $A$ | 2.394(−3) | 1.625(−2) | 6.794(−2) | 2.177(−1) |
| $A'$ | 2.322(−3) | 1.588(−2) | 6.677(−2) | 2.156(−1) |
| $A''$ | 2.236(−3) | 1.546(−2) | 6.537(−2) | 2.117(−1) |
| $A'''$ | 2.293(−3) | 1.574(−2) | 6.630(−2) | 2.143(−1) |
| $^3P_1$–$^1P_1$ (M1) | | | | |
| $E^e$ | 22 398 | 30 031 | 37 050 | 43 757 |
| $E^R$ | 22 681 | 30 299 | 37 312 | 44 026 |
| $M^R$ | −9.350(−9) | −2.101(−8) | −3.859(−8) | −6.335(−8) |
| $M^{NR}$ | −1.410(−10) | −2.397(−10) | −3.277(−10) | −3.079(−10) |
| $A'''$ | 1.740(−3) | 1.188(−2) | 4.968(−2) | 1.593(−1) |
| $^3P_2$–$^1P_1$ (M1) | | | | |
| $E^e$ | 22 274 | 29 770 | 36 582 | 42 995 |
| $E^R$ | 22 556 | 30 036 | 36 841 | 43 262 |
| $M^R$ | 9.179(−9) | 2.064(−8) | 3.783(−8) | 6.187(−8) |
| $M^{NR}$ | 1.407(−10) | 2.393(−10) | 3.282(−10) | 3.076(−10) |
| $A'''$ | 2.779(−3) | 1.893(−2) | 7.859(−2) | 2.489(−1) |
| $^3P_1$–$^1P_1$ (E2) | | | | |
| $E^e$ | 22 398 | 30 031 | 37 050 | 43 757 |
| $E^R$ | 22 681 | 30 299 | 37 312 | 44 026 |
| $M^R$ | −6.835(−9) | −1.136(−8) | −1.696(−8) | −2.354(−8) |
| $M^{NR}$ | −9.450(−10) | −8.305(−10) | −3.909(−10) | −7.807(−11) |
| $A'''$ | 4.159(−4) | 1.795(−3) | 5.509(−3) | 1.309(−2) |
| $^3P_2$–$^1P_1$ (E2) | | | | |
| $E^e$ | 22 274 | 29 770 | 36 582 | 42 995 |
| $E^R$ | 22 556 | 30 036 | 36 841 | 43 262 |
| $M^R$ | 4.632(−9) | 7.161(−9) | 1.025(−8) | 1.358(−8) |
| $M^{NR}$ | 7.481(−10) | 4.836(−10) | −3.585(−11) | −4.295(−10) |
| $A'''$ | 3.010(−4) | 1.196(−3) | 3.497(−3) | 7.630(−3) |

is less important for highly charged ions. The $^3P_1$–$^3P_2$ transition can be either of M1 or E2 type. However, the E2 transition rates are about five orders smaller than those of the M1 transition rates.

Table 5 gives the results for the $LS$ forbidden M1 and E2 transitions. The transition energies, radiative elements and rates are listed for the lowest four ions in the sequence. By comparing the *ab initio* rate $A$ with the finally corrected one $A'''$ it can be found that the difference decreases as the nuclear charge increases. The only exception is the $^3P_2$–$^1P_1$ (E2) transition. Even if the difference of 4% is larger than that for other transitions for the $S^{4+}$ ion it is still less than the deviation of 6% among different strategies in the same transition for the $Al^+$ ion.

**Table 6.** The rates (in $s^{-1}$) of forbidden transitions (M1, E2 and M2) for the Mg-like ions from different calculations.

| | | M1 (3s3p) | | | | | E2 (3s3p) | | M2 |
|---|---|---|---|---|---|---|---|---|---|
| $Z$ | Ref. | $^3P_0$–$^3P_1$ | $^3P_0$–$^1P_1$ | $^3P_1$–$^1P_1$ | $^3P_1$–$^3P_2$ | $^3P_2$–$^1P_1$ | $^3P_0$–$^3P_2$ | $^3P_1$–$^3P_2$ | g–3s3p $^3P_2$ |
| 13 | | 4.061(−6) | 2.293(−3) | 1.740(−3) | 2.565(−5) | 2.779(−3) | 1.857(−10) | 5.663(−11) | 3.413(−3) |
| | [14] | 4.20(−6) | | | 2.31(−5) | | 1.64(−10) | | |
| | [15] | 3.984(−6) | | | 2.522(−5) | | 1.769(−10) | | 3.295(−3) |
| | [11] | 4.24(−6) | 2.88(−3) | 5.7(−1) | 2.67(−5) | 3.51(−3) | | | |
| 14 | | 3.771(−5) | 1.574(−2) | 1.188(−2) | 2.398(−4) | 1.893(−2) | 2.878(−9) | 8.811(−10) | 1.261(−2) |
| | [14] | 3.92(−5) | | | 2.24(−4) | | 2.79(−9) | | |
| | [15] | 3.731(−5) | | | 2.391(−4) | | 2.812(−9) | | 1.221(−2) |
| | [11] | 3.83(−5) | 1.82(−2) | 2.22 | 2.42(−4) | 2.19(−2) | | | |
| 15 | | 2.103(−4) | 6.630(−2) | 4.968(−2) | 1.386(−3) | 7.857(−2) | 2.499(−8) | 7.779(−9) | 3.248(−2) |
| | [14] | 2.24(−4) | | | 1.31(−3) | | 2.36(−8) | | |
| | [15] | 2.115(−4) | | | 1.377(−3) | | 2.453(−8) | | 3.167(−2) |
| | [11] | 2.12(−4) | 7.8(−2) | 6.3 | 1.39(−3) | 9.2(−2) | | | |
| 16 | | 9.069(−4) | 2.143(−1) | 1.593(−1) | 5.963(−3) | 2.489(−1) | 1.542(−7) | 4.818(−8) | 6.827(−2) |
| | [11] | 8.53(−4) | 2.36(−1) | 1.40(1) | 6.10(−3) | 2.73(−1) | | | |
| 17 | | 3.107(−3) | 5.910(−1) | 4.357(−1) | 2.117(−2) | 6.704(−1) | 7.463(−7) | 2.373(−7) | 1.256(−1) |
| | [11] | 3.04(−3) | 6.2(−1) | 2.78(1) | 2.13(−2) | 7.0(−1) | | | |
| 18 | | 9.265(−3) | 1.430 | 1.044 | 6.496(−2) | 1.576 | 3.033(−6) | 9.795(−7) | 2.120(−1) |
| | [11] | 9.39(−3) | 1.34 | 4.88(1) | 6.41(−2) | 1.47 | | | |
| 20 | | 6.025(−2) | 6.558 | 4.679 | 4.539(−1) | 6.725 | 3.477(−5) | 1.167(−5) | 5.055(−1) |
| | [11] | 6.01(−2) | 7.5 | 1.58(2) | 4.59(−1) | 7.7 | | | |
| 26 | | 3.541 | 2.093(2) | 1.355(2) | 3.779(1) | 1.514(2) | 8.923(−3) | 3.556(−3) | 3.389 |
| | [10] | 3.32 | 1.90(2) | | 3.80(1) | 1.40(2) | 9.0(−3) | 3.6(−3) | 3.39 |

**Table 7.** The energies (in $cm^{-1}$) and rates (in $s^{-1}$) of the E1 and M2 transitions for the Mg-like ions calculated with strategy IV. No QED corrections have been included. The line next to $Z = 13$–16 gives the corresponding experimental energies and the rates with proper correction.

| | $3s^2\ ^1S_0$–$3s3p\ ^3P_1$ (E1) | | | $3s^2\ ^1S_0$–$3s3p\ ^1P_1$ (E1) | | | $3s^2\ ^1S_0$–$3s3p\ ^3P_2$ (M2) | |
|---|---|---|---|---|---|---|---|---|
| $Z$ | $\Delta E$ | $A_B$ | $A_C$ | $\Delta E$ | $A_B$ | $A_C$ | $\Delta E$ | $A$ |
| 13 | 37 543 | 3.104(3) | 3.262(3) | 60 224 | 1.417(9) | 1.437(9) | 37 668 | 3.454(−3) |
| | 37 454 | 3.067(3) | | 59 852 | 1.391(9) | | 37 578 | 3.413(−3) |
| 14 | 52 886 | 1.658(4) | 1.720(4) | 83 185 | 2.480(9) | 2.509(9) | 53 149 | 1.265(−2) |
| | 52 853 | 1.645(4) | | 82 884 | 2.453(9) | | 53 114 | 1.261(−2) |
| 15 | 68 137 | 5.812(4) | 6.064(4) | 105 449 | 3.649(9) | 3.685(9) | 68 608 | 3.248(−2) |
| | 68 139 | 5.790(4) | | 105 189 | 3.622(9) | | 68 607 | 3.248(−2) |
| 16 | 83 357 | 1.597(5) | 1.704(5) | 127 382 | 4.906(9) | 4.950(9) | 84 121 | 6.813(−2) |
| | 83 394 | 1.603(5) | | 127 151 | 4.879(9) | | 84 155 | 6.827(−2) |
| 17 | 98 595 | 3.763(5) | 4.044(5) | 149 185 | 6.239(9) | 6.294(9) | 99 758 | 1.256(−1) |
| 18 | 113 880 | 7.952(5) | 8.540(5) | 170 976 | 7.643(9) | 7.709(9) | 115 569 | 2.120(−1) |
| 20 | 144 676 | 2.819(6) | 3.008(6) | 214 829 | 1.065(10) | 1.075(10) | 147 907 | 5.055(−1) |
| 22 | 175 909 | 8.045(6) | 8.520(6) | 259 450 | 1.396(10) | 1.407(10) | 181 528 | 1.036 |
| 24 | 207 699 | 1.972(7) | 2.083(7) | 305 275 | 1.759(10) | 1.773(10) | 216 839 | 1.932 |
| 26 | 240 162 | 4.306(7) | 4.524(7) | 352 774 | 2.163(10) | 2.180(10) | 254 298 | 3.389 |
| 29 | 290 276 | 1.171(8) | 1.225(8) | 428 298 | 2.865(10) | 2.885(10) | 315 590 | 7.324 |
| 35 | 396 266 | 5.500(8) | 5.725(8) | 601 972 | 4.799(10) | 4.829(10) | 463 946 | 3.021(1) |
| 36 | 414 680 | 6.778(8) | 7.040(8) | 634 939 | 5.221(10) | 5.253(10) | 492 988 | 3.799(1) |
| 41 | 509 870 | 1.633(9) | 1.692(9) | 823 517 | 8.019(10) | 8.057(10) | 662 692 | 1.187(2) |
| 42 | 529 515 | 1.891(9) | 1.958(9) | 866 850 | 8.760(10) | 8.799(10) | 702 333 | 1.491(2) |
| 47 | 630 719 | 3.511(9) | 3.633(9) | 1 119 169 | 1.389(11) | 1.393(11) | 936 131 | 4.696(2) |
| 54 | 781 238 | 6.594(9) | 6.821(9) | 1 601 355 | 2.800(11) | 2.803(11) | 1 391 269 | 2.389(3) |
| 60 | 919 868 | 9.878(9) | 1.022(10) | 2 178 673 | 5.342(11) | 5.344(11) | 1 943 753 | 9.728(3) |
| 70 | 1175 922 | 1.665(10) | 1.725(10) | 3 627 905 | 1.658(12) | 1.658(12) | 3 347 937 | 9.956(4) |
| 74 | 1288 977 | 1.989(10) | 2.061(10) | 4 437 583 | 2.634(12) | 2.634(12) | 4 138 378 | 2.491(5) |
| 79 | 1440 257 | 2.443(10) | 2.534(10) | 5 692 862 | 4.705(12) | 4.706(12) | 5 368 708 | 7.726(5) |
| 82 | 1536 609 | 2.745(10) | 2.851(10) | 6 600 254 | 6.663(12) | 6.667(12) | 6 260 691 | 1.511(6) |
| 92 | 1888 482 | 3.905(10) | 4.052(10) | 10 716 550 | 2.107(13) | 2.110(13) | 10 323 600 | 1.351(7) |

To the best of our knowledge, there are no experimental measurements of the M1, E2, M2 forbidden transitions for the Mg iso-electronic sequence. In table 6, the present calculations are compared with other theoretical results. The present results are in good agreement with the earlier MCDHF calculations [15] for the transitions between the fine structure levels of $3s3p\ ^3P$ and for the M2 transition of $3s^2$–$3s3p\ ^3P_2$. Compared with recent second-order relativistic MBPT calculations, the differences range from 3% to 13% for the transitions between fine structure levels. For the $Fe^{14+}$ ion, the present rates agree with those from the relativistic self-consistent-field method of Anderson [10] to within 10%. Compared with the 1951 calculations of Naqvi [11], in which the empirical term intervals and transformation coefficients were used to account for the effect of configuration interaction, most results are in reasonable agreement except for the $^3P_1$–$^1P_1$ M1 transition. For that transition, the discrepancy is about two orders along the whole sequence. The reason for this is unclear. The three M1 transitions, $^3P_1$–$^1P_1$, $^3P_0$–$^1P_1$ and $^3P_2$–$^1P_1$, are all from $^3P$–$^1P$. The present results are of the same order but those of Naqvi differ by about two orders of magnitude. The $^3P_1$ state may mix with the $^1P_1$ state but the $^1P_1$–$^1P_1$ M1 transition is also $LS$ forbidden because of $\Delta J = 0$ [12].

**Table 8.** The QED influence on the energies (in $cm^{-1}$) and the rates (in $s^{-1}$) of the E1 and M2 transitions for Mg-like ions. $\Delta E^e$ represents the experimental energy. $\Delta E^C$ is the theoretical value with QED and mass polarization corrections. $A$ indicates the *ab initio* transition rate (in $s^{-1}$) and $A_N$ is the value normalized with the experimental energy or with $\Delta E^C$ when the experimental energy is not available. The rate of the Babushkin gauge is adopted for the E1 transitions.

| | $3s^2\ ^1S_0$–$3s3p\ ^3P_1$ (E1) | | | | $3s^2\ ^1S_0$–$3s3p\ ^1P_1$ (E1) | | | | $3s^2\ ^1S_0$–$3s3p\ ^1P_1$ (M2) | | | |
|---|---|---|---|---|---|---|---|---|---|---|---|---|
| $Z$ | $\Delta E^e$ | $\Delta E^C$ | $A$ | $A_N$ | $\Delta E^e$ | $\Delta E^C$ | $A$ | $A_N$ | $\Delta E^e$ | $\Delta E^C$ | $A$ | $A_N$ |
| 17 | 97 958 | 98 515 | 3.763(5) | 3.691(5) | 148 949 | 149 103 | 6.239(9) | 6.209(9) | 99 123 | 99 680 | 1.256(−1) | 1.217(−1) |
| | 98 700[a] | | | 3.775(5) | | | | | | | | |
| 18 | 113 904 | 113 770 | 7.952(5) | 7.957(5) | 170 722 | 170 864 | 7.643(9) | 7.609(9) | 115 585 | 115 462 | 2.120(−1) | 2.121(−1) |
| 20 | 144 675 | 144 487 | 2.819(6) | 2.819(6) | 214 482 | 214 637 | 1.065(10) | 1.060(10) | 147 912 | 147 724 | 5.055(−1) | 5.056(−1) |
| 22 | 175 753 | 175 610 | 8.045(6) | 8.024(6) | 258 973 | 259 149 | 1.396(10) | 1.388(10) | 181 400 | 181 240 | 1.036 | 1.032 |
| 24 | 207 400 | 207 253 | 1.972(7) | 1.963(7) | 304 630 | 304 829 | 1.759(10) | 1.748(10) | 216 590 | 216 412 | 1.932 | 1.921 |
| 26 | 239 660 | 239 528 | 4.306(7) | 4.279(7) | 351 914 | 352 143 | 2.163(10) | 2.147(10) | 253 820 | 253 692 | 3.389 | 3.357 |
| 29 | 289 401 | 289 265 | 1.171(8) | 1.160(8) | 426 987 | 427 301 | 2.865(10) | 2.839(10) | 314 753 | 314 631 | 7.324 | 7.227 |
| 35 | 394 255 | 394 077 | 5.500(8) | 5.417(8) | | 599 857 | 4.799(10) | 4.748(10) | 462 216 | 461 896 | 3.021(1) | 2.965(1) |
| 36 | 412 290 | 412 226 | 6.778(8) | 6.661(8) | 632 187 | 632 575 | 5.221(10) | 5.153(10) | 490 722 | 490 694 | 3.799(1) | 3.712(1) |
| 41 | | 505 762 | 1.633(9) | 1.594(9) | | 819 622 | 8.019(10) | 7.906(10) | | 658 890 | 1.187(2) | 1.153(2) |
| 42 | 525 028 | 525 000 | 1.891(9) | 1.843(9) | 862 140 | 862 583 | 8.760(10) | 8.618(10) | 698 188 | 698 162 | 1.491(2) | 1.448(2) |
| 47 | | 623 735 | 3.511(9) | 3.396(9) | | 1 112 652 | 1.389(11) | 1.365(11) | | 929 728 | 4.696(2) | 4.538(2) |
| 54 | | 769 370 | 6.594(9) | 6.298(9) | | 1 590 416 | 2.800(11) | 2.743(11) | | 1 380 465 | 2.389(3) | 2.298(3) |
| 60 | | 902 209 | 9.878(9) | 9.320(9) | | 2 162 487 | 5.342(11) | 5.224(11) | | 1 927 717 | 9.728(3) | 9.333(3) |
| 70 | | 1144 516 | 1.665(10) | 1.535(10) | | 3 599 130 | 1.658(12) | 1.619(12) | | 3 319 340 | 9.956(4) | 9.538(4) |
| 74 | | 1250 393 | 1.989(10) | 1.816(10) | | 4 402 130 | 2.634(12) | 2.571(12) | | 4 103 115 | 2.491(5) | 2.387(5) |
| 79 | | 1391 174 | 2.443(10) | 2.202(10) | | 5 647 477 | 4.705(12) | 4.593(12) | | 5 323 531 | 7.726(5) | 7.406(5) |
| 82 | | 1480 384 | 2.745(10) | 2.455(10) | | 6 547 952 | 6.663(12) | 6.506(12) | | 6 208 609 | 1.511(6) | 1.449(6) |
| 92 | | 1802 883 | 3.905(10) | 3.398(10) | | 10 634 596 | 2.107(13) | 2.059(13) | | 10 241 915 | 1.351(7) | 1.298(7) |

[a] C E Moore 1971 *Atomic Energy Levels*.

Since the NR limit correction and singlet–triplet normalization have less effect on highly charged ions we calculated the ions above $S^{+4}$ in an *ab initio* way. The energies and rates of the E1 and M2 transitions are shown in table 7 for the Mg-like ions calculated with strategy IV. The line next to $Z = 13$–16 gives the corresponding experimental energies and the normalized rates. For the resonance transition of $3s^2\ ^1S_0$–$3s3p\ ^1P_1$ the rates from the Babushkin gauge and Coulomb gauge agree to within 0.1–1.4%. As the nuclear charge increases the agreement becomes better. For the intercombination transition of $3s^2\ ^1S_0$–$3s3p\ ^3P_1$ the rates from different gauges are within 3.5–7.5% of each other. As the nuclear charge increases, the difference does not decrease but remains constant at about 3.7%. That may be attributed to the effect of the negative continuum [13, 14]. The rate of the magnetic quadrupole transition $3s^2\ ^1S_0$–$3s3p\ ^3P_2$ (M2) is very small for the $Al^+$ ion but it rises rapidly with the increasing nuclear charge. It reaches $10^7\ s^{-1}$ for the $U^{80+}$ ion.

Although the NR limit correction and singlet–triplet separation normalization are less important for the high-$Z$ ions, the QED effects become significant. A comparison is shown in table 8 for both the energy and rate. The vacuum polarization, mass polarization and finite-nucleus effect are included and the self-energy correction is treated perturbatively. The self-energy correction for each orbital is obtained by

$$E_{SE} = \frac{D(\mathrm{MCDHF})}{D(\mathrm{H})}\alpha^5 Z^4 F_{n\kappa}(\alpha Z)/\pi n^3$$

where $D(\mathrm{MCDHF})$ and $D(\mathrm{H})$ are the charge density of the MCDHF orbital and hydrogenic orbital integrated from the origin to 0.3 Compton wavelength [16]. The function $F_{n\kappa}(\alpha Z)$ for the $n \leqslant 2$ orbitals is obtained by interpolating in or extrapolating from the hydrogenic values of Mohr [17]. For the $n \geqslant 3$ orbitals in the s or p symmetry, the function is calculated by scaling the hydrogenic values. For the other orbitals, the function is estimated by using a series expansion [18].

The difference between the experimental energy ($\Delta E^e$) from the NIST Database [19] and the present one $\Delta E$ in table 7 without the QED correction increases rapidly with the nuclear charge. At $Z = 42$, it reaches more than 4000 $cm^{-1}$ or about 1% for all three transitions. However, with the QED correction the difference for the intercombination transition reduces to 100–220 $cm^{-1}$ or 0.01–0.1% for $Z = 18$–42. The only exception is for $Z = 17$ where the present energy with the QED correction differs from that of the NIST Database by 550 $cm^{-1}$, but only by 200 $cm^{-1}$ from that of Moore's tables. For the resonance transition, the difference between the experimental and computational energy increases from 130 to 420 $cm^{-1}$ with

**Table 9.** The total contribution of QED and mass polarization to the transition energies (in $cm^{-1}$) for the $Cu^{17+}$, $Mo^{30+}$ and $U^{80+}$ ions.

| | $Cu^{17+}$ | | $Mo^{30+}$ | | $U^{80+}$ |
|---|---|---|---|---|---|
| Trans. | Present | [20] | Present | [20] | Present |
| $3s^2$–$^3P_1$ | −1010 | −1042 | −4514 | −4563 | −85 599 |
| $3s^2$–$^3P_2$ | −959 | | −4171 | | −81 685 |
| $3s^2$–$^1P_1$ | −996 | −1021 | −4267 | −4288 | −81 954 |
| $^3P_0$–$^3P_1$ | 15 | | 28 | | −40 |
| $^3P_0$–$^3P_2$ | 66 | | 372 | | 3 874 |
| $^3P_0$–$^1P_1$ | 29 | | 276 | | 3 605 |
| $^3P_1$–$^3P_2$ | 51 | | 344 | | 3 914 |
| $^3P_1$–$^1P_1$ | 14 | | 248 | | 3 645 |
| $^3P_2$–$^1P_1$ | −37 | | −96 | | −269 |

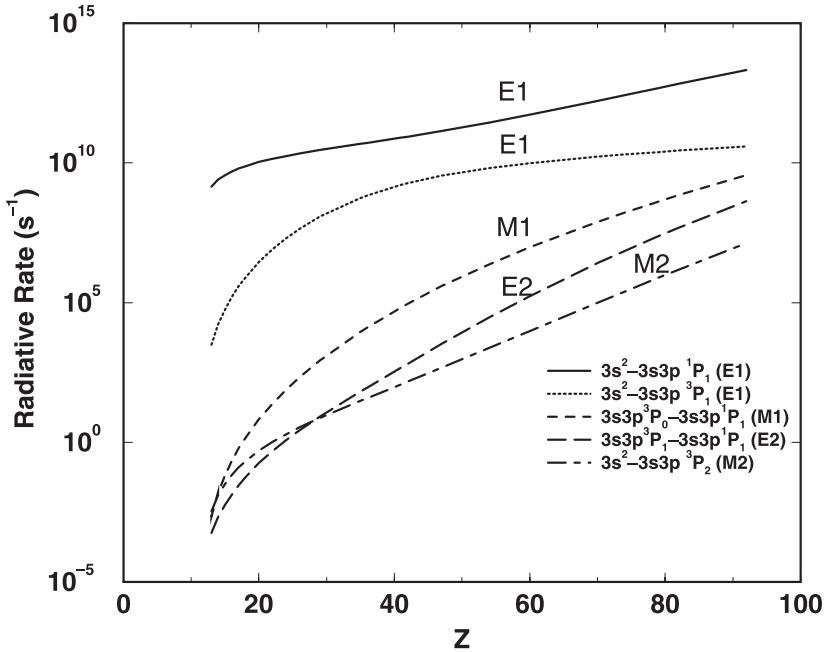


**Figure 1.** The radiative rates of typical E1, M1, E2 and M2 transitions as functions of the nuclear charge for the Mg iso-electronic sequence.

respect to the nuclear charge increasing from 17 to 42. This may be attributed to the residual correlation effects. The QED influence on the transition rate is taken into account by using equation (6). In table 8 $A_N$ is the value normalized with the experimental energy or with the corrected theoretical energy $\Delta E^C$ when the experimental energy is not available. The rate of the Babushkin gauge is adopted for the E1 transitions. By comparing the *ab initio* rate ($A$) with the normalized one ($A_N$) in table 8, it can be found that the effect of the transition energy normalization is very small for the low-$Z$ ions but increases for the higher-$Z$ ions. For $Z = 42$, it reduces the rates by about 3%, 2% and 3% for the intercombination, resonance and M2 transitions, respectively. The effect is more significant for the intercombination transition as the nuclear charge increases but remains constant at about 2% and 4% for the resonance and M2 transition, respectively. For $Z = 92$ the effect for the intercombination transition becomes as large as 14% since the QED correction is relatively large for the transition energy.

The total contribution of QED and mass polarization to the transition energies is given in table 9 for the $Cu^{17+}$, $Mo^{30+}$ and $U^{80+}$ ions. The present results agree with those of the *ab initio* calculation of Chen and Cheng [20] for the $Cu^{17+}$ and $Mo^{30+}$ ions. It is also seen that the contribution to the energy of the transition between the 3s3p states is small. It suggests that a transition energy normalization should be unnecessary for such transitions.

The rates of the magnetic dipole transitions are shown in table 10. The transitions are very weak for the light ions, but they rise dramatically with increasing nuclear charge. At the high-$Z$ end it can be noted that the transitions can be divided into weak and intense groups. Using the $jj$ notation, one can identify that the weak group includes transitions of the same relativistic configurations, namely $3s_{1/2}3p_{1/2}$ or $3s_{1/2}3p_{3/2}$, and the intense group includes the transitions between the two configurations.

In table 11 the rates of the electric quadrupole transitions are listed for the sequence. The agreement between the Babushkin and the Coulomb gauge is very poor for the spin-changing

**Table 10.** The energies (in $cm^{-1}$) and rates (in $s^{-1}$) of the M1 transitions between the 3s3p $^3P_{0,1,2}$, 3s3p $^1P_1$ levels for the Mg-like ions calculated with strategy IV. The line next to $Z = 13$–16 gives the corresponding experimental energies and the rates with the proper correction.

| | $^3P_0$–$^3P_1$ | | $^3P_0$–$^1P_1$ | | $^3P_1$–$^1P_1$ | | $^3P_1$–$^3P_2$ | | $^3P_2$–$^1P_1$ | |
|---|---|---|---|---|---|---|---|---|---|---|
| $Z$ | $\Delta E$ | $A$ | $\Delta E$ | $A$ | $\Delta E$ | $A$ | $\Delta E$ | $A$ | $\Delta E$ | $A$ |
| 13 | 61.43 | 4.169(−6) | 22 743 | 2.394(−3) | 22 681 | 1.817(−3) | 125.1 | 2.639(−5) | 22 556 | 2.902(−3) |
| | 60.88 | 4.061(−6) | 22 459 | 2.293(−3) | 22 398 | 1.740(−3) | 123.9 | 2.565(−5) | 22 274 | 2.779(−3) |
| 14 | 128.9 | 3.851(−5) | 30 428 | 1.625(−2) | 30 299 | 1.226(−2) | 263.6 | 2.469(−4) | 30 036 | 1.955(−2) |
| | 128.6 | 3.771(−5) | 30 159 | 1.574(−2) | 30 031 | 1.188(−2) | 261.7 | 2.398(−4) | 29 770 | 1.893(−2) |
| 15 | 229.3 | 2.169(−4) | 37 542 | 6.794(−2) | 37 312 | 5.091(−2) | 471.5 | 1.413(−3) | 36 841 | 8.051(−2) |
| | 227.4 | 2.103(−4) | 37 277 | 6.630(−2) | 37 050 | 4.968(−2) | 468.4 | 1.386(−3) | 36 582 | 7.857(−2) |
| 16 | 369.1 | 9.040(−4) | 44 395 | 2.177(−1) | 44 026 | 1.619(−1) | 764.0 | 6.013(−3) | 43 262 | 2.530(−1) |
| | 369.5 | 9.069(−4) | 44 126 | 2.143(−1) | 43 757 | 1.593(−1) | 761.9 | 5.963(−3) | 42 995 | 2.489(−1) |
| 17 | 557.0 | 3.107(−3) | 51 146 | 5.910(−1) | 50 589 | 4.357(−1) | 1 162 | 2.117(−2) | 49 427 | 6.704(−1) |
| 18 | 801.8 | 9.265(−3) | 57 898 | 1.430 | 57 096 | 1.044 | 1 689 | 6.496(−2) | 55 407 | 1.576 |
| 20 | 1 497 | 6.025(−2) | 71 650 | 6.558 | 70 153 | 4.679 | 3 230 | 4.539(−1) | 66 922 | 6.725 |
| 22 | 2 525 | 2.887(−1) | 86 066 | 2.398(1) | 83 541 | 1.664(1) | 5 620 | 2.387 | 77 922 | 2.240(1) |
| 24 | 3 951 | 1.104 | 101 527 | 7.504(1) | 97 576 | 5.038(1) | 9 140 | 1.025(1) | 88 436 | 6.241(1) |
| 26 | 5 832 | 3.541 | 118 444 | 2.093(2) | 112 612 | 1.355(2) | 14 136 | 3.779(1) | 98 476 | 1.514(2) |
| 29 | 9 588 | 1.561(1) | 147 610 | 8.317(2) | 138 022 | 5.079(2) | 25 314 | 2.153(2) | 112 708 | 4.659(2) |
| 35 | 20 466 | 1.474(2) | 226 172 | 8.851(3) | 205 706 | 4.824(3) | 67 680 | 3.991(3) | 138 026 | 2.531(3) |
| 36 | 22 666 | 1.989(2) | 242 924 | 1.264(4) | 220 258 | 6.776(3) | 78 308 | 6.138(3) | 141 951 | 3.172(3) |
| 41 | 34 867 | 6.947(2) | 348 514 | 6.619(4) | 313 647 | 3.327(4) | 152 822 | 4.372(4) | 160 824 | 8.184(3) |
| 42 | 37 487 | 8.554(2) | 374 822 | 9.016(4) | 337 336 | 4.491(4) | 172 818 | 6.262(4) | 164 518 | 9.595(3) |
| 47 | 51 077 | 2.063(3) | 539 526 | 3.857(5) | 488 449 | 1.863(5) | 305 411 | 3.289(5) | 183 038 | 1.896(4) |
| 54 | 70 623 | 5.124(3) | 890 739 | 2.378(6) | 820 116 | 1.135(6) | 610 030 | 2.454(6) | 210 086 | 3.936(4) |
| 60 | 87 334 | 9.279(3) | 1346 139 | 9.648(6) | 1258 805 | 4.619(6) | 1023 885 | 1.106(7) | 234 920 | 6.484(4) |
| 70 | 114 884 | 2.005(4) | 2566 867 | 7.770(7) | 2451 984 | 3.764(7) | 2172 015 | 9.914(7) | 279 968 | 1.284(5) |
| 74 | 125 852 | 2.596(4) | 3274 458 | 1.670(8) | 3148 606 | 8.128(7) | 2849 400 | 2.192(8) | 299 205 | 1.629(5) |
| 79 | 139 582 | 3.488(4) | 4392 187 | 4.152(8) | 4252 606 | 2.032(8) | 3928 451 | 5.604(8) | 324 154 | 2.148(5) |
| 82 | 147 847 | 4.113(4) | 5211 491 | 7.022(8) | 5063 644 | 3.446(8) | 4724 082 | 9.605(8) | 339 562 | 2.512(5) |
| 92 | 175 703 | 6.769(4) | 9003 768 | 3.677(9) | 8828 064 | 1.818(9) | 8435 118 | 5.203(9) | 392 947 | 4.044(5) |

**Table 11.** The energies (in $cm^{-1}$) and rates (in $s^{-1}$) of the E2 transitions between the 3s3p $^3P_{0,1,2}$, 3s3p $^1P_1$ levels for the Mg-like ions calculated with strategy IV. The line next to $Z = 13$–16 gives the corresponding experimental energies and the rates with proper correction.

| | $^3P_0$–$^3P_2$ | | | $^3P_1$–$^1P_1$ | | | $^3P_1$–$^3P_2$ | | | $^3P_2$–$^1P_1$ | | |
|---|---|---|---|---|---|---|---|---|---|---|---|---|
| $Z$ | $\Delta E$ | $A_B$ | $A_C$ | $\Delta E$ | $A_B$ | $A_C$ | $\Delta E$ | $A_B$ | $A_C$ | $\Delta E$ | $A_B$ | $A_C$ |
| 13 | 186.5 | 1.944(−10) | 2.054(−10) | 22 681 | 5.826(−4) | 7.164(−4) | 125.1 | 5.938(−11) | 6.277(−11) | 22 556 | 4.436(−4) | 7.573(−4) |
| | 184.8 | 1.857(−10) | | 22 398 | 4.159(−4) | | 123.9 | 5.663(−11) | | 22 274 | 3.010(−4) | |
| 14 | 392.5 | 3.009(−9) | 3.058(−9) | 30 299 | 2.149(−3) | 2.432(−3) | 263.6 | 9.255(−10) | 9.416(−10) | 30 036 | 1.411(−3) | 2.136(−3) |
| | 390.3 | 2.878(−9) | | 30 031 | 1.795(−3) | | 261.7 | 8.811(−10) | | 29 770 | 1.196(−3) | |
| 15 | 700.8 | 2.591(−8) | 2.616(−8) | 37 312 | 5.900(−3) | 6.206(−3) | 471.5 | 8.041(−9) | 8.128(−9) | 36 841 | 3.547(−3) | 4.426(−3) |
| | 695.8 | 2.499(−8) | | 37 050 | 5.509(−3) | | 468.4 | 7.779(−9) | | 36 582 | 3.497(−3) | |
| 16 | 1 133 | 1.557(−7) | 1.576(−7) | 44 026 | 1.342(−2) | 1.198(−2) | 764.0 | 4.886(−8) | 4.934(−8) | 43 262 | 7.310(−3) | 6.002(−3) |
| | 1 131 | 1.542(−7) | | 43 757 | 1.309(−2) | | 761.9 | 4.818(−8) | | 42 995 | 7.630(−3) | |
| 17 | 1 719 | 7.463(−7) | 7.551(−7) | 50 589 | 2.878(−2) | 2.715(−2) | 1 162 | 2.373(−7) | 2.398(−7) | 49 427 | 1.516(−2) | 1.367(−2) |
| 18 | 2 491 | 3.033(−6) | 3.057(−6) | 57 096 | 5.655(−2) | 5.532(−2) | 1 689 | 9.795(−7) | 9.866(−7) | 55 407 | 2.851(−2) | 2.760(−2) |
| 20 | 4 727 | 3.477(−5) | 3.500(−5) | 70 153 | 1.809(−1) | 1.816(−1) | 3 230 | 1.167(−5) | 1.174(−5) | 66 922 | 8.146(−2) | 8.192(−2) |
| 22 | 8 144 | 2.798(−4) | 2.808(−4) | 83 541 | 4.907(−1) | 4.977(−1) | 5 620 | 9.850(−5) | 9.887(−5) | 77 922 | 1.926(−1) | 1.966(−1) |
| 24 | 13 091 | 1.743(−3) | 1.748(−3) | 97 576 | 1.193 | 1.209 | 9 140 | 6.497(−4) | 6.386(−4) | 88 436 | 3.971(−1) | 4.026(−1) |
| 26 | 19 968 | 8.923(−3) | 8.943(−3) | 112 612 | 2.685 | 2.717 | 14 136 | 3.556(−3) | 3.565(−3) | 98 476 | 7.351(−1) | 7.441(−1) |
| 29 | 34 902 | 7.803(−2) | 7.806(−2) | 138 022 | 8.247 | 8.379 | 25 314 | 3.486(−2) | 3.490(−2) | 112 708 | 1.578 | 1.605 |
| 35 | 88 146 | 2.896 | 2.894 | 205 706 | 6.502(1) | 6.531(1) | 67 680 | 1.673 | 1.656 | 138 026 | 4.614 | 4.636 |
| 36 | 100 973 | 4.927 | 4.924 | 220 258 | 9.078(1) | 9.148(1) | 78 308 | 2.972 | 2.970 | 141 951 | 5.276 | 5.297 |
| 41 | 187 689 | 5.588(1) | 5.584(1) | 313 647 | 4.740(2) | 4.771(2) | 152 822 | 4.129(1) | 4.126(1) | 160 824 | 8.941 | 8.959 |
| 42 | 210 305 | 8.731(1) | 8.724(1) | 337 336 | 6.579(2) | 6.621(2) | 172 818 | 6.694(1) | 6.688(1) | 164 518 | 9.709 | 9.726 |
| 47 | 356 488 | 6.931(2) | 6.926(2) | 488 449 | 3.327(3) | 3.347(3) | 305 411 | 6.244(2) | 6.238(2) | 183 038 | 1.355(1) | 1.356(1) |
| 54 | 680 653 | 8.805(3) | 8.801(3) | 820 116 | 2.957(4) | 2.973(4) | 610 030 | 9.347(3) | 9.339(3) | 210 086 | 1.877(1) | 1.877(1) |
| 60 | 1111 219 | 6.053(4) | 6.052(4) | 1258 805 | 1.727(5) | 1.736(5) | 1023 885 | 7.070(4) | 7.065(4) | 234 920 | 2.327(1) | 2.326(1) |
| 70 | 2286 899 | 1.035(6) | 1.035(6) | 2451 984 | 2.584(6) | 2.597(6) | 2172 015 | 1.336(6) | 1.336(6) | 279 968 | 3.139(1) | 3.136(1) |
| 74 | 2975 252 | 2.911(6) | 2.913(6) | 3148 606 | 7.067(6) | 7.102(6) | 2849 400 | 3.862(6) | 3.862(6) | 299 205 | 3.497(1) | 3.493(1) |
| 79 | 4068 033 | 9.952(6) | 9.959(6) | 4252 606 | 2.358(7) | 2.368(7) | 3928 451 | 1.356(7) | 1.356(7) | 324 154 | 3.976(1) | 3.971(1) |
| 82 | 4871 929 | 2.020(7) | 2.022(7) | 5063 644 | 4.735(7) | 4.755(7) | 4724 082 | 2.789(7) | 2.789(7) | 339 562 | 4.280(1) | 4.277(1) |
| 92 | 8610 821 | 1.882(8) | 1.884(8) | 8828 064 | 4.317(8) | 4.334(8) | 8435 118 | 2.683(8) | 2.685(8) | 392 947 | 5.372(1) | 5.379(1) |

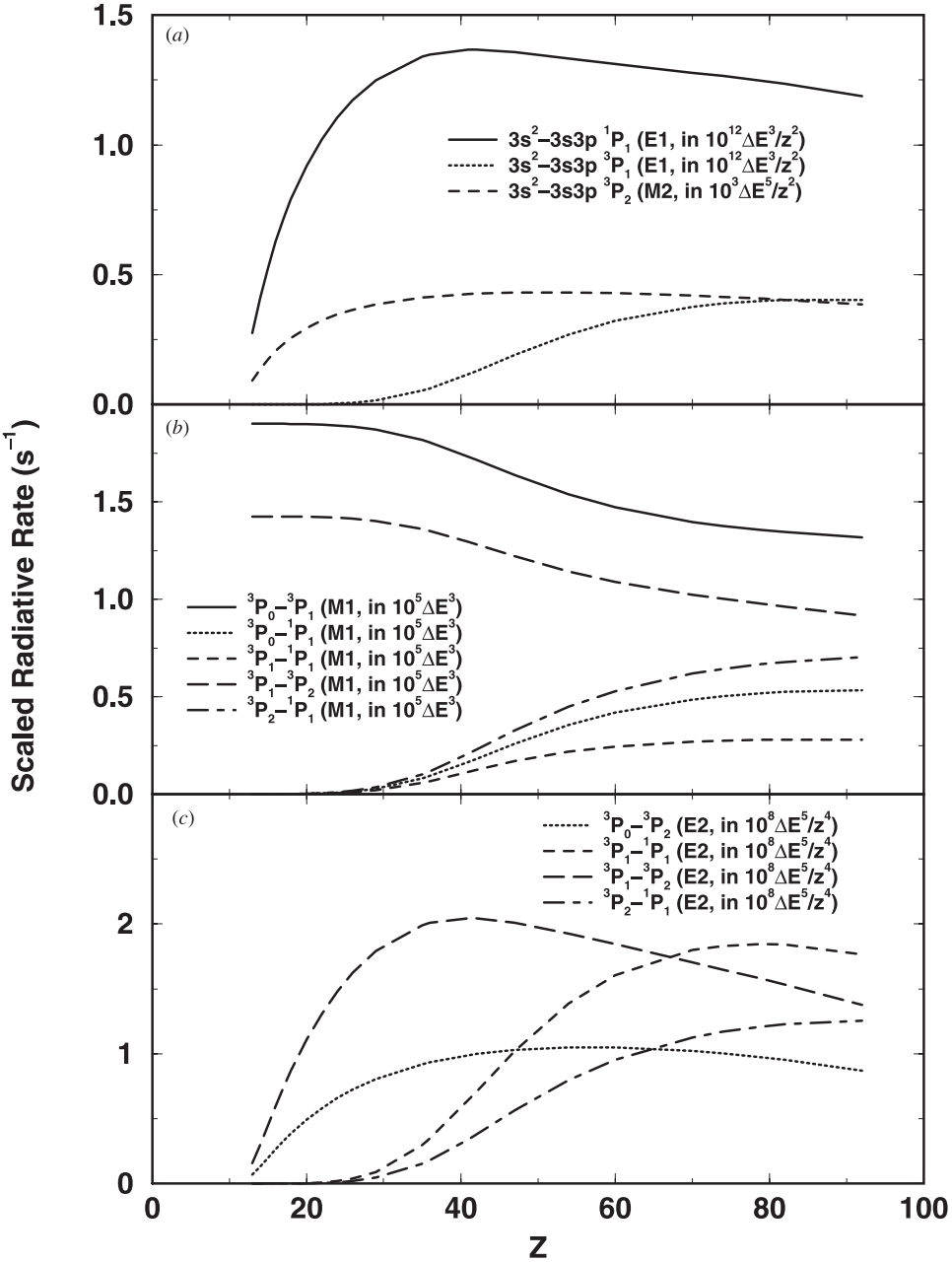


**Figure 2.** The scaled radiative transition rates for the Mg iso-electronic sequence. (*a*) E1- and M2-type transitions, (*b*) M1 transitions and (*c*) E2 transitions. The scaling parameter $z = Z - 11$, is an approximation to the effective nuclear charge.

transitions at the low-$Z$ end. However, as $Z$ increases the agreement improves quickly. At the high-$Z$ end one can find a similar situation as in M1 that the intra-configuration transition is quite weak and those of inter-configuration are intense.

Figure 1 shows the rates as functions of $Z$ for typical E1, M1, E2 and M2 transitions. It can be seen that the forbidden transition rates increase more rapidly with respect to the increasing nuclear charge than the allowed transition rate does, especially in the low-$Z$ region. The spin forbidden E1 transition (intercombination) is an exception. Although increasing rapidly in the low-$Z$ region, it slows down from about $Z = 40$. At $Z = 92$, the M1 transition rate approaches that of the spin forbidden E1 transition. In the low-$Z$ region the $^3P_1$–$^1P_1$ E2 transition is weaker than the $3s^2\ ^1S_0$–$3s3p\ ^3P_2$ M2 transition. This is primarily because the $^3P_1$–$^1P_1$ E2 transition is $LS$ forbidden and it depends strongly on the spin–orbit interaction. As $Z$ increases, the $^3P_1$–$^1P_1$ E2 transition is enhanced and crosses the $3s^2\ ^1S_0$–$3s3p\ ^3P_2$ M2 transition at about $Z = 30$. At the high-$Z$ region the rates in decreasing order are E1 resonance, E1 intercombination, M1, E2 and M2 as expected.

In tables 8, 10 and 11, the transition rates vary extensively with respect to the nuclear charge, especially the forbidden transitions. A general scaling formula of

$$A^e(\kappa) = \bar{A}^e(\kappa)\Delta E^{(2\kappa+1)}/z^{2\kappa}$$
$$A^m(\kappa) = \bar{A}^m(\kappa)\Delta E^{(2\kappa+1)}/z^{2(\kappa-1)}$$

may be introduced to reduce the intensity for electric and magnetic multipole transitions, where $z = Z - 11$ is the spectroscopic symbol of the ion. The scaled radiative rates are shown in figure 2. The scaled values vary smoothly with respect to the nuclear charge in the high-$Z$ region. In the low-$Z$ region, the scaled rates of the $LS$ allowed transitions vary quickly but still with good behaviour. The behaviour may be improved by using a more precise effective atomic charge instead of the spectroscopic symbol. The rates of the $LS$ forbidden transitions in this region vary extensively because they depend on the mixing of the $^1P_1$ and $^3P_1$ components. This mixing varies with respect to the nuclear charge, which is not described in the general scaling formula.

In summary, the forbidden transitions between the $3s^2\ ^1S_0, 3s3p\ ^3P_{0,1,2}, ^1P_1$ states for the Mg-like ions are investigated using the MCDHF approach. The resonance and intercombination transitions of $3s^2\ ^1S_0$–$3s3p\ ^{1,3}P_1$ are also calculated. The fine structure splittings from different optimization strategies become identical after the NR offset is subtracted. For the $LS$ allowed transitions which have non-zero rates at the NR limit, the radiative matrix elements are stable with respect to the optimization strategy but the transition energies vary for different strategies. For the $LS$ forbidden transitions, the NR limit correction, transition energy and singlet–triplet normalization are necessary for the lower charged ions. A general scaling formula can be used to reduce the extensive variation of transition rates with respect to the nuclear charge.

## Acknowledgments

The authors are grateful to Professor Y-K Kim for helpful discussions on the QED effects. This work was supported by the Chemical Sciences, Geosciences and Biosciences Division, Office of Basic Energy Sciences, Office of Science, US Department of Energy.

## References

[1] Träbert E 2000 *Phys. Scr.* **61** 257
[2] Zou Y and Froese Fischer C 2000 *Phys. Rev.* A **62** 062505
[3] Kim Y K, Parente F, Marques J P, Indelicato P and Desclaux J P 1998 *Phys. Rev.* A **58** 1885
[4] Tachiev G and Froese Fischer C 1999 *J. Phys. B: At. Mol. Opt. Phys.* **32** 5805
[5] Fleming J, Hibbert A and Stafford R P 1994 *Phys. Scr.* **49** 316

[6] Parpia F A, Froese Fischer C and Grant I P 1996 *Comput. Phys. Commun.* **94** 249
[7] Malmqvist P Å 1986 *Int. J. Quantum Chem.* **30** 479
[8] Olsen J, Godefroid M R, Jönsson P, Malmqvist P Å and Froese Fischer C 1995 *Phys. Rev.* E **52** 4499
[9] Grant I P 1974 *J. Phys. B: At. Mol. Phys.* **7** 1458
[10] Anderson E K and Anderson E M 1983 *Opt. Spectrosk.* **55** 500
[11] Naqvi A M 1951 *Thesis* Harvard University
[12] Martin W C and Wiese W L 1996 *Atomic, Molecular and Optical Physics Handbook* ed G W F Drake (New York: AIP) p 146
[13] Safronova U I, Johnson W R and Berry H G 2000 *Phys. Rev.* A **61** 052503-1
[14] Safronova U I 2000 *Mol. Phys.* **98** 1213
[15] Jönsson P and Froese Fischer C 1997 *J. Phys. B: At. Mol. Opt. Phys.* **30** 5861
[16] Kim Y K, Baik D H, Indelicato P and Desclaux J P 1991 *Phys. Rev.* A **44** 148
[17] Mohr P J 1983 *At. Data Nucl. Data Tables* **29** 453
[18] Klarsfeld S and Maquet A 1973 *Phys. Lett.* B **43** 201
[19] NIST Database http://physics.nist.gov/cgi-bin/AtData/levels_form
[20] Chen M H and Cheng K T 1997 *Phys. Rev.* A **55** 3440